J. Fluid Mech. (1983), *vol.* 137, *pp.* 307–329
Printed in Great Britain

The production of turbulent stress in a shear flow by irrotational fluctuations

By I. S. GARTSHORE,
The University of British Columbia, Vancouver, B.C., Canada

P. A. DURBIN
NASA (Lewis), Cleveland, Ohio, U.S.A.

AND J. C. R. HUNT
Department of Applied Mathematics and Theoretical Physics, Silver Street, Cambridge CB3 9EW, England

(Received 26 January 1983 and in revised form 31 August 1983)

This paper is a study of how external turbulence affects an initially turbulence-free region in which there is a mean-velocity gradient $\mathrm{d}U/\mathrm{d}z$. Rapid-distortion theory shows how external turbulence induces irrotational fluctuations in the sheared region, which interact with the shear to produce rotational velocity fluctuations and mean Reynolds stresses. These stresses extend into the sheared region over a distance of the order of the integral scale L_∞. Since the actual front between the initial external turbulence and the shear flow is a randomly contorted surface, the turbulence of a fixed point near the front is intermittent. Intermittency is included in the present analysis by a simple statistical model.

Experiments were done in a wind tunnel with the flow divided by a plate extending from upstream to $x = 0$. Above the plate, turbulence was produced by a grid. Below the plate a low turbulence shear was produced by wire screens. The wake of the plate ($x > 0$) decayed downstream.

Turbulent shear stress was observed to grow from zero to significant values in the interaction region. The magnitude and extent of the observed stress agrees reasonably well with predictions. We conclude that turbulent stresses can be produced by irrotational fluctuations in a region of mean shear, and that this effect can be estimated using rapid-distortion theory.

1. Introduction

An irrotational flow field, such as that associated with a single vortex or multiple vortices, can produce additional turbulence and mixing in a nearby region of mean shear, such as a boundary layer. Vortex generators which are used to delay separation in adverse pressure gradients use this principle (see Lachmann 1961). The mechanism involved is conceptually simple: the isolated vortex sketched in figure 1 deflects the vortex lines of the nearby shear region so that they can be stretched by the velocity gradient and thereby draw energy from the mean motion. As a result, strong streamwise vorticity can be created in the shear region by re-orientation of the original cross-stream vorticity. Additional mixing occurs, and the new streamwise vorticity can repeat the process in nearby regions of mean shear. The original mean shear would in general be altered by the interaction, which is nonlinear and

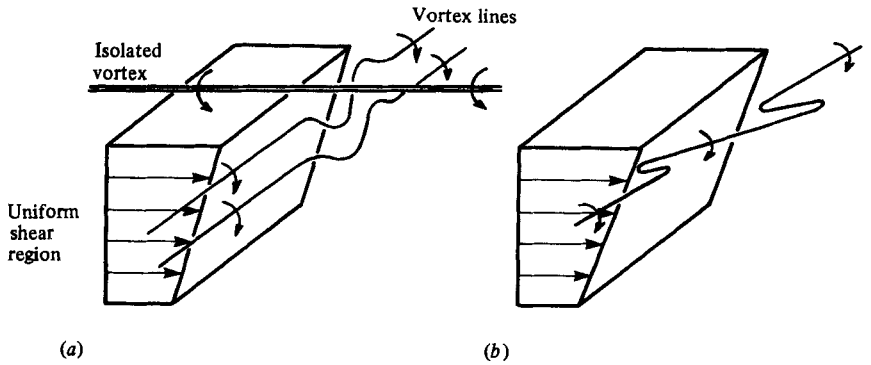

FIGURE 1. Conceptual sketch of interaction between an isolated vortex and a nearby region of uniform shear: (*a*) initial effect of an isolated vortex on other vortex lines; (*b*) subsequent effect of shear on a typical vortex line.

complicated as recent measurements show (Mehta, Shabaka & Bradshaw 1981). If the effect of the isolated vortex is weak, however, and the interaction is brief, linearized approximations may be used to estimate the effects involved.

The isolated vortex of figure 1 may be thought of as one element in a three-dimensional unsteady field of vorticity representing freestream turbulence near a region of mean shear. In this case the irrotational motion associated with the turbulence can be estimated, at least in a region far from a boundary of the vorticity (Phillips 1955; Bradshaw 1967). One well-known result is that the irrotational fluctuation energy decreases as z^{-4}, where z is measured normal to the turbulence boundary, assumed to be plane. With the irrotational flow field associated with the turbulence known, estimates can be made of its interaction with a nearby region of mean shear. Durbin (1978) has previously reported such an extension of Phillips' analysis. He also considered the case where the sheared region is bounded by a plane wall; turbulence near a plane boundary was analysed in detail by Hunt & Graham (1978). The present analysis is another example of this class of problems involving plane boundaries and (stable) parallel shear flows to which RDT can be applied (Goldstein 1979).

Here we examine the interaction between a turbulent region of approximately constant mean velocity and an adjacent region which is initially non-turbulent, or of very low turbulence, but has an approximately constant mean-velocity gradient. Rapid-distortion theory is applied to this problem in §2, and an experimental examination of the interaction is described in §3. Comparisons and conclusions follow in §4.

2. The application of rapid-distortion theory

The initial development of turbulence induced in a shear flow by an adjacent turbulent region can be analysed by making the approximations of rapid-distortion theory. We show how shear-layer turbulence grows in intensity by extracting energy from the mean shear and how Reynolds shear stresses are produced in the process. Two cases are considered:

case (*i*): a plane turbulent layer bounds a region of uniform shear (figure 2*a*);

case (*ii*): a plane turbulent layer bounds a region of non-uniform shear (figure 2*b*).

Present interest is in the evolution with time of turbulence in the shear layer. In case

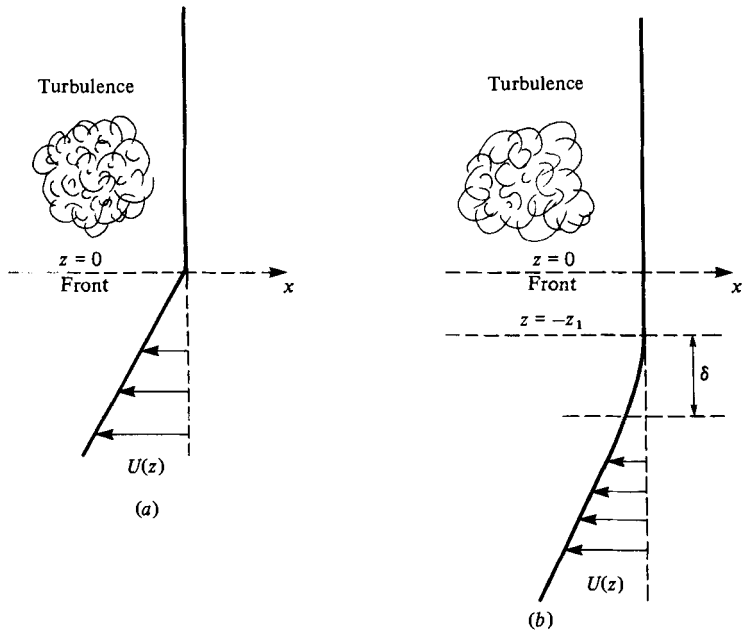

FIGURE 2. Idealized flow fields assumed in the rapid-distortion-theory calculations: (*a*) case (i); (*b*) case (ii).

(ii) the analysis is restricted to asymptotically short times, but the behaviour of the turbulence above the shear layer is also considered.

Case (i)

First consider the field of turbulence induced in a region of uniform shear by a random normal velocity at its boundary $z = 0$ (see figure 2*a*). In the present experiments the shear flow is bounded by the turbulent wake of a splitter plate (see §§3 and 4). The velocity at the edge of this wake is supposed known, and the turbulence induced by this velocity is calculated.

In the 'rapid-distortion' approach the essential assumptions are that the advection and straining of vorticity by turbulent velocities is weak compared with that by the mean velocity and its local gradients (for which a *sufficient* condition in this case is that $u_\infty \ll L\,\mathrm{d}U/\mathrm{d}z$), and that the time t for the distortion is small compared with the Lagrangian timescale L/u_∞ (Hunt 1973). (Townsend (1976) has shown that in shear flows the theory agrees with measurements of turbulence correlation function even when $t\,\mathrm{d}U/\mathrm{d}z$ is as large as 2.) Then the linearized inviscid equations of incompressible fluid flow may be used. Let $U(z)$ be the mean velocity and $\boldsymbol{u} = (u, v, w)$ be the turbulent velocity.

Taking the curl of the momentum equations and using the fact that $\mathrm{d}^2U/\mathrm{d}z^2 = 0$, we obtain

$$\left.\begin{aligned} \frac{\mathrm{D}}{\mathrm{D}t}\left(\frac{\partial w}{\partial y} - \frac{\partial v}{\partial z}\right) &= \frac{\mathrm{d}U}{\mathrm{d}z}\frac{\partial v}{\partial x} \quad \text{(i)}, \\ \frac{\mathrm{D}}{\mathrm{D}t}\left(\frac{\partial u}{\partial z} - \frac{\partial w}{\partial x}\right) &= \frac{\mathrm{d}U}{\mathrm{d}z}\frac{\partial v}{\partial y} \quad \text{(ii)}, \end{aligned}\right\} \tag{1a}$$

where

$$\frac{\mathrm{D}}{\mathrm{D}t} = \frac{\partial}{\partial t} + U(z)\frac{\partial}{\partial x}.$$

Using the continuity equation

$$\frac{\partial u}{\partial x} + \frac{\partial v}{\partial y} + \frac{\partial w}{\partial z} = 0, \tag{1b}$$

it follows from taking the curl of (1*a*) that

$$\frac{\mathrm{D}}{\mathrm{D}t}\nabla^2 w = 0. \tag{1c}$$

Then if the initial flow is irrotational, it follows that for all subsequent time

$$\nabla^2 w = 0. \tag{1d}$$

The v-component of velocity can be obtained from (1*a*(i)) once the solution for w is found from (1*d*), and u can then be obtained from (1*b*).

The effect of the upper turbulent region (figure 2) on the lower shear flow is simplified by supposing that $w(x, y, z = 0) = A(x, y)$, where $A(x, y)$ is a known, spatially homogeneous random function. (Actually, we are using Taylor's hypothesis to remove any time dependence of A: we have adopted locally a frame of reference moving at the mean velocity at $z = 0$, which is why the shear flow below $z = 0$ in figure 2 is in the negative x-direction.) The approximation that $A(x, y)$ is homogeneous in the x-direction is justified because the wake thickness changes very little in a distance typical of the turbulence scale.

Introducing the 2-dimensional Fourier transforms in the x- and y-directions in which the turbulence is homogeneous,

$$\begin{aligned} \hat{u}(k, l(z)) &= \iint_{-\infty}^{\infty} \mathrm{e}^{\mathrm{i}(kx+ly)}\, u(x, y, z)\, \mathrm{d}y\, \mathrm{d}x, \\ \hat{A}(k, l) &= \iint_{-\infty}^{\infty} \mathrm{e}^{\mathrm{i}(kx+ly)}\, A(x, y)\, \mathrm{d}y\, \mathrm{d}x, \end{aligned} \tag{2}$$

into (1) simplifies their solution.† For the vertical velocity, since $\hat{w} \to 0$ as $z \to -\infty$,

$$\hat{w} = \hat{A}\, \mathrm{e}^{\kappa z}, \tag{3}$$

where

$$\kappa^2 = k^2 + l^2.$$

If a lower boundary, where $\hat{w} = 0$, exists, the result (3) can be modified following Hunt & Graham (1978) and Durbin (1978).

A two-dimensional spectrum of the function $\hat{A}$ is assumed for computational convenience to have the form:

$$\overline{|\hat{A}|^2} = \frac{u_\infty^2 \kappa^2 L_\infty^4\, \mathrm{e}^{-\kappa L_\infty}}{12\pi}, \tag{4}$$

where u_∞ and L_∞ are velocity and length scales:

$$u_\infty^2 = \iint_{-\infty}^{\infty} \overline{|\hat{A}|^2}\, \mathrm{d}k\, \mathrm{d}l, \quad L_\infty = \frac{3\pi \int_{-\infty}^{\infty} \overline{|\hat{A}|^2_{l=0}}\, \mathrm{d}k}{u_\infty^2}.$$

† Note the difference between this and the analysis of homogeneous shear flow where three dimensional Fourier transforms are used and the wavenumber m in the z-direction is a function of strain and k (Townsend 1976).

$\overline{|\hat{A}|^2}$ has been given an axisymmetric form, and it satisfies $\lim_{\kappa\to 0}\overline{|\hat{A}|^2} = O(\kappa^2)$ in order to be consistent with the constraint $\lim_{k\to 0} E(k) = O(k^4)$, usually imposed on the three-dimensional energy spectrum of homogeneous turbulence.

From (3) and (4)

$$\overline{|\hat{w}|^2} = \frac{u_\infty^2 L_\infty^4 \kappa^2 \mathrm{e}^{-\kappa L_\infty + 2\kappa z}}{12\pi}. \tag{5}$$

Since spectra and variances are related by

$$\overline{u^2} = \iint_{-\infty}^{\infty} \overline{|\hat{u}|^2}\,\mathrm{d}k\,\mathrm{d}l \tag{6}$$

it follows from (5) that

$$\overline{w^2} = \frac{u_\infty^2}{(1+2|z/L_\infty|)^4}. \tag{7}$$

This reproduces Phillips' (1955) asymptotic result $\overline{w^2}\to O(z^{-4})$ as $z\to\infty$.

The equations (1) show that within the shear layer the horizontal components of velocity are driven entirely by the vertical component. Thus the solution (3), along with the condition that initially the velocity is irrotational, completely determines $\hat{u}$ and $\hat{v}$. The initial condition can be written

$$\hat{u} = -\frac{\mathrm{i}k\hat{A}\,\mathrm{e}^{Kz}}{\kappa}, \quad \hat{v} = -\frac{\mathrm{i}l\hat{A}\,\mathrm{e}^{\kappa z}}{\kappa} \tag{8}$$

at $t = 0$. From (6) and (8) $\overline{u^2}(z, t=0) = \overline{v^2}(z, t=0) = \frac{1}{2}\overline{w^2}(z)$. At subsequent times $\overline{u^2}$ and $\overline{v^2}$ will be modified by effects of the mean shear.

Solving (1) by introducing Fourier transforms and substituting the result for $\hat{u}$ into (6) gives

$$\begin{aligned}\overline{u^2} &= \frac{L_\infty^4 u_\infty^2}{12\pi}\iint_{-\infty}^{\infty} \mathrm{e}^{-\kappa L_\infty + 2\kappa z\kappa^2}\left\{\frac{k^2}{\kappa^2} + \left(\frac{l^4}{k^2\kappa^4 z^2} + \frac{l^2}{\kappa^3 z}\right)(2 - 2\cos(kz_1 T))\right\}\mathrm{d}k\,\mathrm{d}l \\ &= \tfrac{1}{2}\overline{w^2}(z) + \tfrac{1}{6}L_\infty^4 u_\infty^2 \int_0^\infty \kappa^3 \mathrm{e}^{-\kappa L_\infty + 2\kappa z}\left(\frac{g_1(\kappa z T)}{\kappa^2 z^2} + \left(1 - \frac{2J_1(\kappa z T)}{\kappa z T}\right)\Big/\kappa z\right)\mathrm{d}\kappa,\end{aligned} \tag{9}$$

where $T = t\,\mathrm{d}U/\mathrm{d}z$ is non-dimensional time, J_1 is a Bessel function and

$$\begin{aligned} g_1(\alpha) &\equiv \frac{2}{\pi}\int_0^\pi \frac{\sin^4\phi}{\cos^2\phi}(1 - \cos(\alpha\cos\phi))\,\mathrm{d}\phi \\ &= 2\alpha\, g(\alpha) - 3 + \frac{2J_1(\alpha)}{\alpha} + 2J_0(\alpha); \end{aligned} \tag{10}$$

with

$$g(\alpha) \equiv \frac{1}{\pi}\int_0^\pi \frac{1-\cos(\alpha\cos\phi)}{\alpha\cos^2\phi}\,\mathrm{d}\phi. \tag{11}$$

The function $g(\alpha)$ was analysed by Durbin (1978), who showed that

$$g(\alpha)\to\tfrac{1}{2}\alpha + O(\alpha^3) \quad (\alpha\to 0),$$

$$g(\alpha)\to 1 + O(\alpha^{-\frac{3}{2}}) \quad (\alpha \gg 1)$$

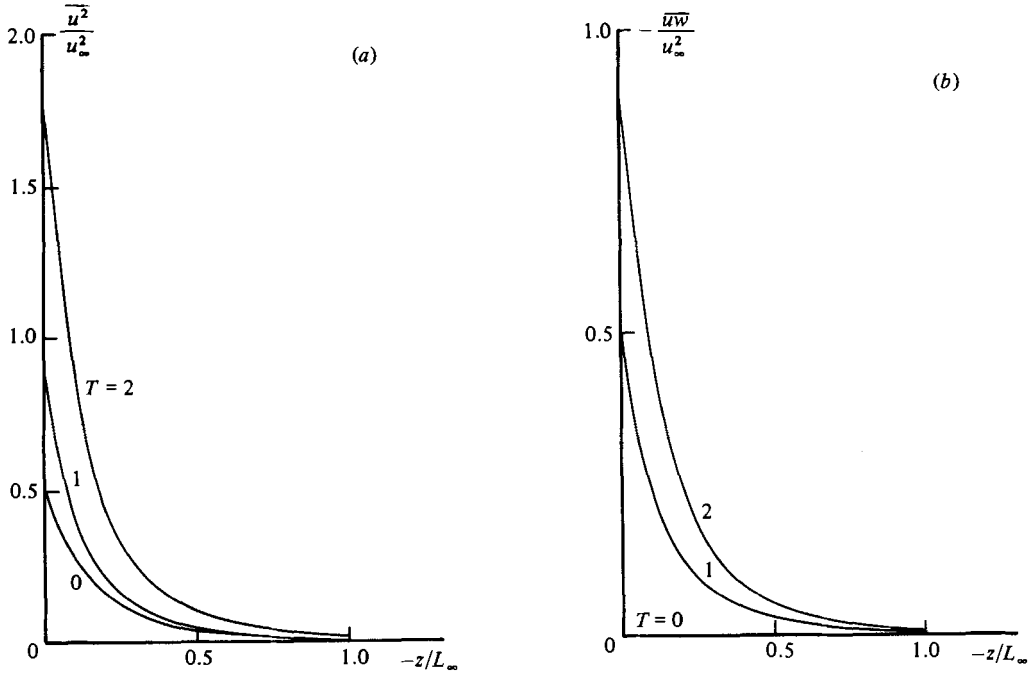

FIGURE 3. Calculated distributions of Reynolds stress near the plane boundary of a turbulent field for various strain ratios T: (*a*) longitudinal normal stress; (*b*) shear stress.

(the latter limit is taken to indicate the trend when $\alpha \geqslant 1$). From these it follows that

$$\left.\begin{aligned} &\left.\begin{aligned} &\overline{u^2} \to \tfrac{1}{2}u_\infty^2 + \tfrac{3}{8}u_\infty^2 T^2, \\ &\overline{v^2} \to \tfrac{1}{2}u_\infty^2 + \tfrac{1}{8}u_\infty^2 T^2 \end{aligned}\right\} \quad \text{as} \quad z \to 0 \quad \text{with} \quad T = O(1) \\ &\overline{u^2} \to \frac{2u_\infty^2 T}{3|z/L_\infty|\,(1+2|z/L_\infty|)^3} \quad \text{for} \quad T \gg 1 \quad \text{with} \quad \frac{z}{L_\infty} = O(1). \end{aligned}\right\} \tag{12}$$

Thus, initially $\overline{u^2}$ grows like T^2, and at large times it grows linearly with T. The mean shear is the source for this growth of the energy of induced turbulence. It also follows from (9) that $\overline{u^2} \sim 1/z^4$ as $z \to -\infty$ for all T; of course the proportionality here is a function of T.

The full expression (9) has been evaluated numerically and is shown in figure 3(*a*). The variance of the initial irrotational velocity field is

$$\overline{u^2} = \tfrac{1}{2}\overline{w^2} = \frac{\tfrac{1}{2}u_\infty^2}{(1+2|z/L_\infty|)^4}.$$

This is subsequently amplified by the mean shear.

The Reynolds stress is found to be

$$\overline{uw} = \frac{u_\infty^2 L_\infty^4}{6}\int_0^\infty \frac{\kappa^2}{z} e^{2\kappa z - \kappa L_\infty}\, g(\kappa z T)\, d\kappa, \tag{13}$$

with $g(\alpha)$ as given above in (11). Asymptotically

$$\left.\begin{aligned} &\overline{uw} \to -\tfrac{1}{2}u_\infty^2 T \quad \text{as} \quad z \to 0 \quad \text{with} \quad T = O(1), \\ &\overline{uw} \to -\frac{u_\infty^2}{3|z/L_\infty|\,(2|z/L_\infty|+1)^3} \quad \text{for} \quad T \gg 1 \quad \text{with} \quad \frac{z}{L_\infty} = O(1). \end{aligned}\right\} \tag{14a}$$

At $T = 0$, $-\overline{uw} \equiv 0$: it grows with time as in figure 3(*b*), in which numerical evaluations of (13) are plotted.

It is instructive to consider these results in terms of the turbulence kinetic energy equation in its linearized form for this problem:

$$\frac{1}{2}\frac{\mathrm{d}\overline{(u^2+v^2+w^2)}}{\mathrm{d}t} = -\overline{uw}\frac{\partial U}{\partial z} - \frac{\partial}{\partial z}(\overline{pw}). \tag{14b}$$

Equations (12) and (14) and also direct calculation show that $\overline{pw} = 0$. This result can also be shown by symmetry arguments: since w for $z < 0$ is independent of $\mathrm{d}U/\mathrm{d}z$, and since $\nabla^2 p = -2\,\mathrm{d}U/\mathrm{d}z\,\partial w/\partial x$, p and $\overline{pw}$ are proportional to $\mathrm{d}U/\mathrm{d}z$. Therefore, since $\overline{pw}$ must be independent of the sign of $\mathrm{d}U/\mathrm{d}z$, $\overline{pw}$ must be zero. However, $\overline{w\,\partial p/\partial x}$ and $\overline{u\,\partial p/\partial z}$ do not have reflectional symmetry about $x = 0$, and therefore are non-zero. These pressure–velocity correlations have an important effect on $\overline{uw}$ in case (ii).

Thus (14*b*) reduces to

$$\frac{1}{2}\frac{\mathrm{d}}{\mathrm{d}t}(\overline{u^2+v^2+w^2}) = -\overline{uw}\,\mathrm{d}U/\mathrm{d}z, \tag{14c}$$

so the increase in kinetic energy is directly proportional to the Reynolds stress. Equations (12) and (14) show that, at large strains, $\overline{u^2} \gg \overline{v^2}$ and that

$$\frac{1}{2}\frac{\mathrm{d}\overline{u^2}}{\mathrm{d}t} \approx -\overline{uw}\frac{\mathrm{d}U}{\mathrm{d}z}.$$

Case (ii)

In the theory presented so far, we have neglected any effects above $z = 0$ of the interactions below $z = 0$. One might expect some irrotational fluctuation in the region $z > 0$, produced by the growth of turbulence below $z \approx 0$. These are of some practical importance if they can produce a Reynolds stress in $z > 0$. The following calculation enables this aspect of the problem to be explored. For simplicity and because the experimental measurements correspond to small-time distortion, we only consider the effects at the beginning of the distortion.

The vertical velocity of the initial rotational turbulence is now specified at the plane $z = 0$, and the mean velocity gradient is imposed at $z < -z_1$. To ensure a continuous matching of the turbulence across $z = -z_1$, the shear increases in an adjustment distance δ: for $\mathrm{d}U/\mathrm{d}z$ we use the form (figure 2*b*)

$$\left.\begin{aligned} \mathrm{d}U/\mathrm{d}z &= \eta U'(z), \\ U' &= 0 \quad (z \geqslant -z_1), \\ U' &= 1 - \mathrm{e}^{(z+z_1)/\delta} \quad (z < -z_1), \end{aligned}\right\} \tag{15}$$

so that η is just the value of $\mathrm{d}U/\mathrm{d}z$ as $z \to -\infty$.

If the turbulent velocity components are expanded as

$$\boldsymbol{u}(x, T) = \boldsymbol{u}^{(0)}(x) + T\boldsymbol{u}^{(1)}(x) + O(T^2),$$

where $T = \eta t$, then $\partial \boldsymbol{u}/\partial T = \boldsymbol{u}^{(1)}(x)$ to lowest order, and $\boldsymbol{u}^{(0)}$ is the initial velocity as given previously in (3) and (8). The pressure must be expanded as $P = \eta p^{(1)} + O(T)$ to be consistent with the expansion of $\boldsymbol{u}$. By the linearized momentum equations $\boldsymbol{u}^{(1)}$ and $p^{(1)}$ satisfy

$$u^{(1)} = -w^{(0)}U' - \frac{\partial p^{(1)}}{\partial x} - \Delta L\frac{\partial u^0}{\partial x}, \quad w^{(1)} = -\frac{\partial p^{(1)}}{\partial z} - \Delta L\frac{\partial w^{(0)}}{\partial x}, \quad \nabla^2 p^{(1)} = -2\frac{\partial w^{(0)}}{\partial x}U'. \tag{16}$$

where $\Delta L = U(z)/\eta$.

The most significant result of the analysis is that when $T \ll 1$ the cospectrum of the Reynolds shear stress is given by

$$\overline{\hat{u}\hat{w}} = \overline{T(\hat{u}^{(0)}\hat{w}^{(1)} + \hat{u}^{(1)}\hat{w}^{(0)}}$$

$$= \begin{cases} \overline{T|\hat{A}|^2}\, \mathrm{e}^{2\kappa z} \dfrac{k^2}{\kappa^2(1+2\kappa\delta)} & (-z_1 \leqslant z \leqslant 0), \\ -T|\hat{A}|^2\, \mathrm{e}^{2\kappa z}\left(\dfrac{l^2}{\kappa^2} - \mathrm{e}^{(z+z_1)}\left(\dfrac{1+2l^2\delta/\kappa}{1+2\kappa\delta}\right)\right) & (z < -z_1). \end{cases}$$

Note that $\overline{\hat{u}\hat{w}}$ is positive in the region between $z = 0$ and $z = -z_1$ where the velocity gradient starts.

Analytical expressions for $\overline{uw}$ can be obtained in the limit of a thin layer between the uniform flow and the velocity gradient (as in our experiment). Thus when $\delta/L_\infty \ll 1$

$$-\overline{uw} = \begin{cases} -\tfrac{1}{2}T\overline{w^{(0)^2}}(z) & (-z_1 < z < 0), \qquad (17a) \\ \tfrac{1}{2}T\overline{w^{(0)^2}}(z)\,(1-2\mathrm{e}^{(z+z_1)/\delta}) & (z < -z_1). \qquad (17b) \end{cases}$$

Equation (17) indicates that initially the *negative* Reynolds shear stress ($-\overline{uw} < 0$) above the shear region is as large as the *positive* Reynolds stress in the shear region $z \ll -z_1$. These stresses of opposite sign connect continuously across a layer below $-z_1$ of thickness $O(\delta)$. Note that $\overline{u^2}$ and $\overline{w^2}$ are only perturbed by $O(T^2)$ (see (12)), and therefore the Reynolds stress increase is the most apparent effect of distortion.

There is a physical explanation for the results in (17) which should give an indication of when this mechanism might be important. Consider the equation for production of Reynolds stress $-\overline{uw}$ in homogeneous turbulent shear flow (dissipation and turbulent-diffusion terms neglected):

$$-\frac{\mathrm{D}\overline{uw}}{\mathrm{D}t} = \underbrace{\overline{w^2}\frac{\mathrm{d}U}{\mathrm{d}z}}_{\mathrm{ST}} + \underbrace{\left(\overline{w\frac{\partial p}{\partial x}} + \overline{u\frac{\partial p}{\partial z}}\right)}_{\mathrm{PV}}. \qquad (18)$$

The shear-turbulence term ST produces Reynolds stress when the w-component of turbulence displaces the vortex lines of the mean flow (cf. figure 1). The pressure term PV is due to rotation and distortion of eddies by the mean velocity gradient: analysis shows that distortion of eddies produces pressure fluctuations which (because they are non-local) cause u and w to become partly in phase with each other. Substituting (17*b*) for $\overline{uw}$ in (18) shows that $\mathrm{PV} = -\frac{1}{2}\mathrm{ST}$. This is different from the result $\mathrm{PV} = -\frac{3}{5}\mathrm{ST}$ given by Townsend (1976) for homogeneous turbulence: the difference is because our result is for non-homogeneous turbulence generated by the irrotational disturbance.

Above the shear layer the first term in (18) is zero. However, the pressure fluctuations extend into the region above $-z_1$ giving $-\mathrm{D}\overline{uw}/\mathrm{D}t = \mathrm{PV} = -\frac{1}{2}\mathrm{ST}$ for the second term. This effectively explains the change of the sign of $\overline{uw}$ in (17) on going from $z < -(z_1+\delta)$ to $z > -z_1$: below the interface, ST causes $-uw$ to be positive; above the interface PV makes it negative.

The Reynolds stress in the unsheared region can also be explained as due to vorticity waves propagating along the interface between the two regions (Durbin 1978). Initially the displacement of the interface produces a u-velocity above $-z_1$ proportional to wT. The associated Reynolds stress is negative and proportional to $-\overline{w^2}T$.

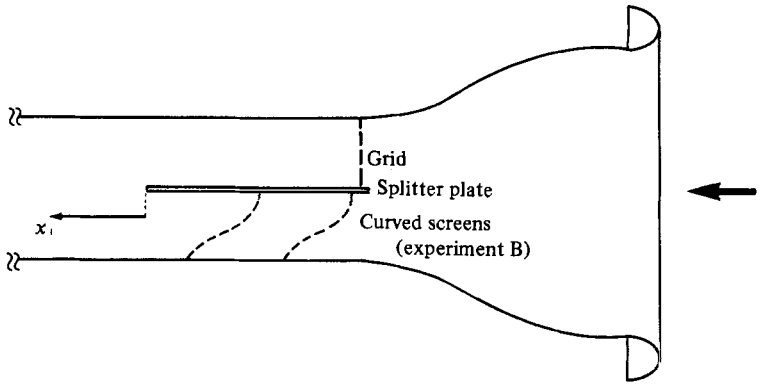

FIGURE 4. Experimental arrangements in the wind tunnel.

The advantages of our short-time analysis are that it clarifies these mechanisms, and that it can be used for more general initial fields of turbulence. However, in comparing with experiment we use the finite-time results of case (i).

3. Experimental arrangements

Measurements of the interaction between grid turbulence, a turbulent wake and an adjacent low turbulent region of uniform shear were made in the DAMTP suction tunnel (Britter, Hunt & Mumford 1979). The arrangement is sketched in figure 4; the tunnel working section, which is 0.46 m square, is divided in half by a horizontal splitter plate 0.61 m long. Above the plate near its leading edge, a uniplanar square-mesh grid with mesh size 58 mm and bar width 14 mm produces grid turbulence. Below the plate, two alternative arrangements were used: for the first set of experiments, designated A, two normal uniform screens were installed to produce a low-intensity stream of uniform velocity and a pressure loss equal to that of the grid above the plate. For the second set of experiments (B) two curved screens were used as shown in figure 4 to produce a region of approximately uniform shear. The two curved screens were identical, their shape being the same as that used by Maull (1969). All screens consisted of 29 SWG wire (0.345 mm diameter) woven in a square mesh with close to one wire per millimetre.

In all experiments, additional plane screens upstream of the splitter plate were used to provide approximately equal mean velocities on either side of the splitter plate wake. The screens for this purpose had different open-area ratios above and below the plate, chosen to create the required effect. Screen open areas were varied by mounting more than one screen together in the same frame and/or by lightly spraying a single screen with paint to increase the effective wire-mesh diameter. Mean velocities in the grid turbulence were approximately 7.6 m/s in all cases. Linearized hot-wire anemometers were used with both normal and slant wires to measure mean velocities and turbulent quantities. Turbulence intensities were low in every position of importance; no longitudinal cooling correction was used in the data reduction.

4. Experimental results

In the first set of experiments (A) the mean velocity outside the splitter plate wake was essentially constant. Profiles at four streamwise positions are shown in figure 5. The wake was initially asymmetric because of different boundary layers on the top

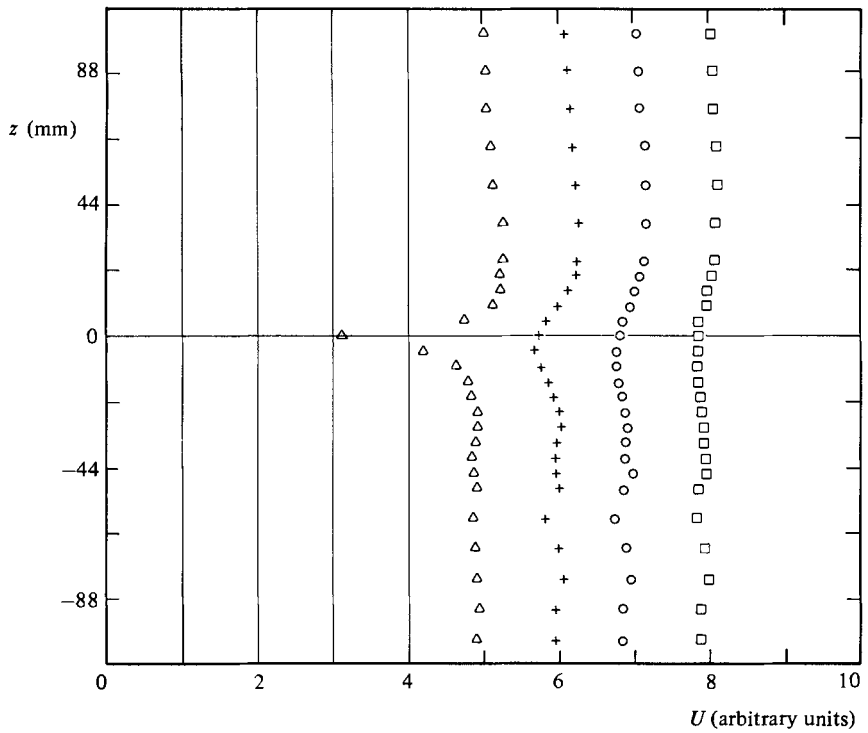

FIGURE 5. Measured mean velocity profiles for experiment A: △, $x = 12$ mm; +, 368 mm; ⊙, 750 mm; ⊡, 1130 mm.

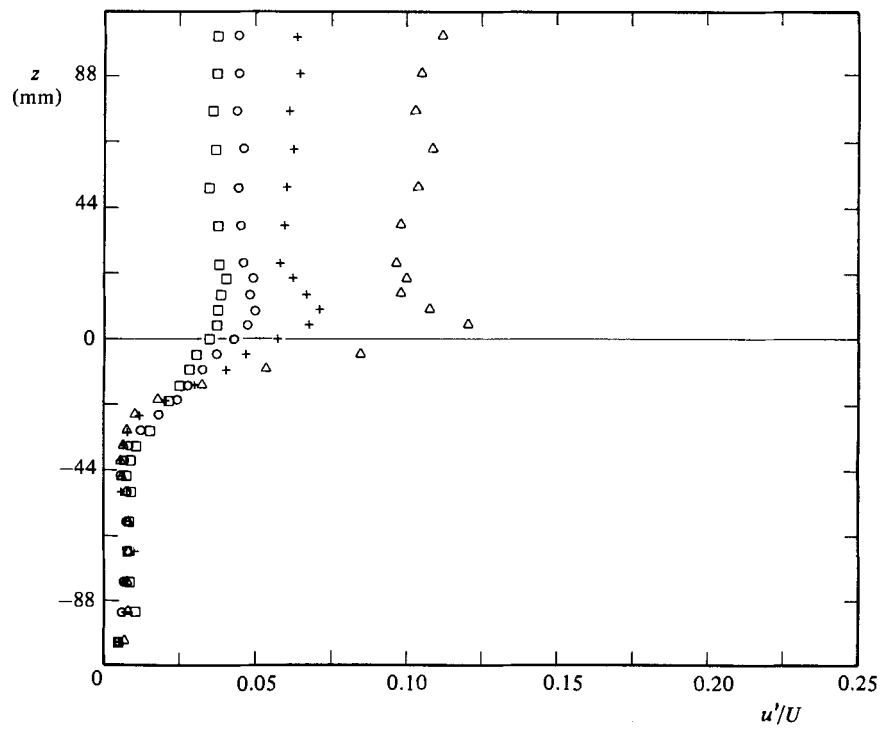

FIGURE 6. Measured distributions of longitudinal turbulence intensity for experiment A; symbols as in figure 5.

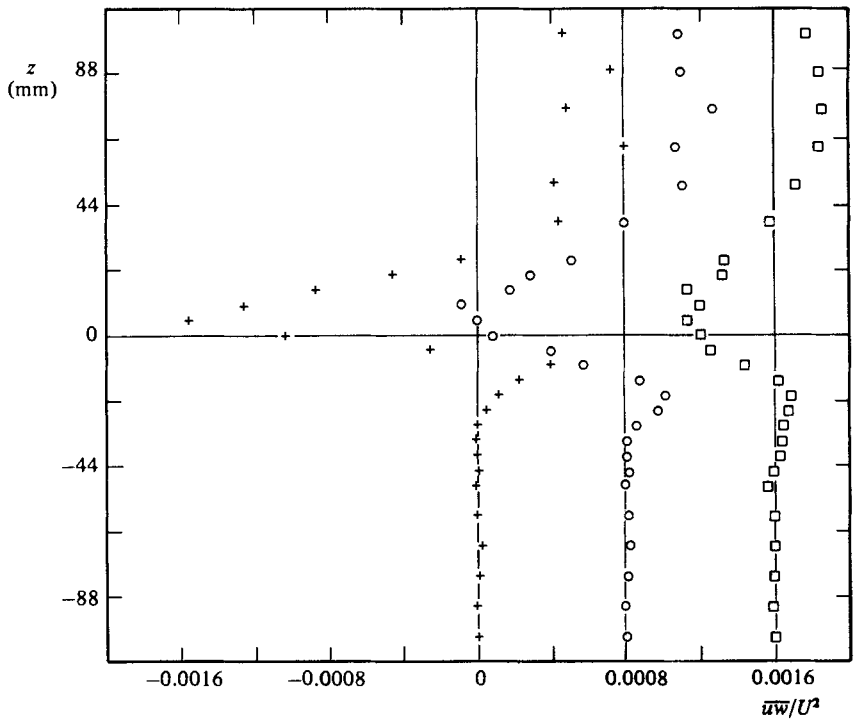

FIGURE 7. Measured turbulence stress for experiment A; symbols as in figure 5.

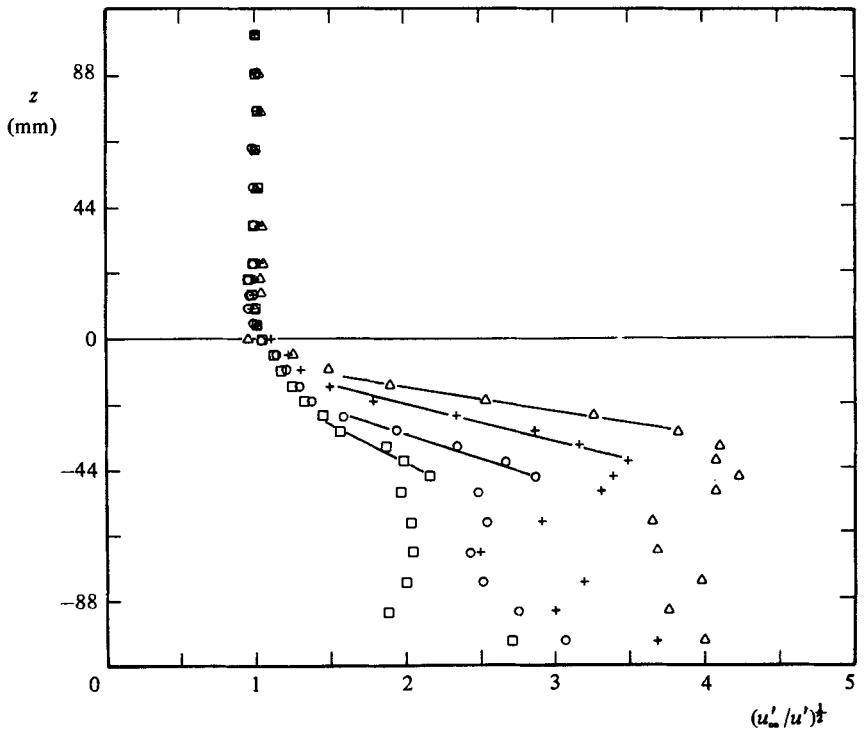

FIGURE 8. Measured turbulence intensity for experiment A plotted to examine Phillips' hypothesis; symbols as in figure 5.

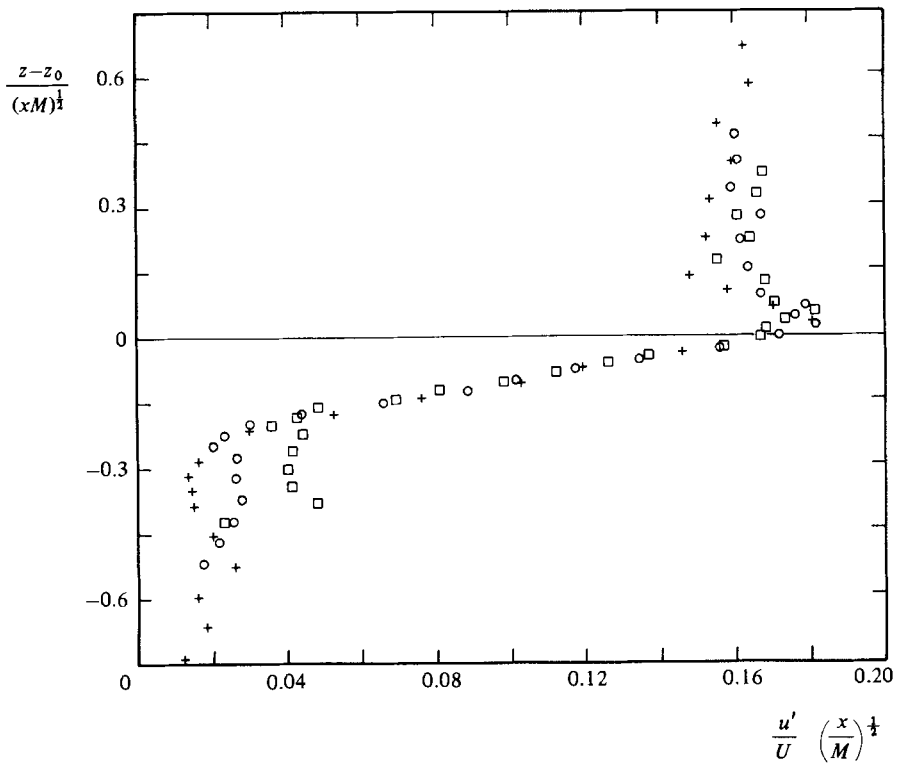

FIGURE 9. Self-similar plot of the longitudinal turbulence intensity measurement of experiment A based on scales appropriate to a small-deficit wake; symbols as in figure 5.

and bottom of the plate, and then developed further asymmetry, because of the turbulence on one side but not on the other. Some evidence of screen non-uniformities can be seen in the slightly uneven mean velocities below the plate (see Castro 1976). Increased velocities can be seen above the plate outside the central wake; these decrease as the flow develops and must be due to the particular grid/boundary connection chosen, a half-mesh opening at each side of the grid, as sketched on the abscissae of figure 5. Longitudinal intensities u' (where the prime denotes the r.m.s. value) at the four locations are shown in figure 6, and shear stresses $-(\overline{uw})$ in figure 7.

The mean velocities of figure 5 show that the wake has a small defect over most of its length. The distributions of turbulence intensity show the expected rapid decrease from their values in the grid turbulence above the wake to about 0.5 % below the wake on the other side. The turbulence intensity in the wake was initially very large, but approached the surrounding grid turbulence values with distance downwind. The shear stress, although somewhat scattered in the grid turbulence region where intensities are high, shows the expected wake-like pattern with positive and negative maxima separated by a point of zero stress near (but not necessarily at) the wake centre as defined by the minimum mean-velocity position. The non-zero stress in the grid-turbulence region must be associated with the mean-velocity variation there, which we have already noted. All stresses decrease in the downstream direction in much the same way since measured values of the stress ratios $\overline{uw}/u'w'$ and w'/u' at

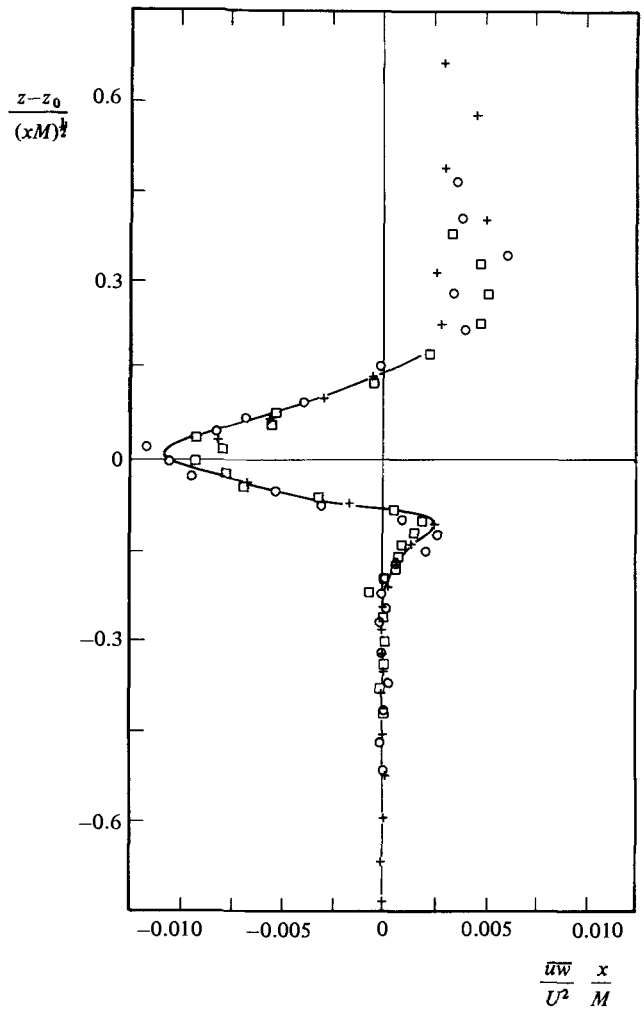

FIGURE 10. Self-similar plot of the shear stress distributions of experiment A based on scales appropriate to a small deficit wake; symbols as in figure 5.

each position are very similar. The maximum negative stress decays very nearly as x^{-1}, as expected for a small deficit wake.

Outside the wake created by the splitter plate, we expect some evidence of irrotational fluctuations appearing on the low turbulence side. Hence a region in which $u' \propto z^{-2}$ should be obtained with z measured from some virtual origin and in a direction normal to the mean flow. This appears in figure 8, in which $(u')^{-\frac{1}{2}}$ is plotted against z; the linear region becomes less well-defined as we proceed downstream. The plots of figure 8 show that the apparent scale of the fluctuations, denoted by the slope or lateral extent of the linear sections, increases as x increases. The increase in scale is more than that due to the increasing scale of the grid turbulence and could therefore be associated with the increasing scale of turbulence in the wake of the splitter plate. This scale change, which should be roughly parabolic with x for a small deficit wake, results in increasingly extensive intermittent regions or increasing wrinkle amplitudes of the so-called 'superlayer' bounding the turbulent wake vorticity. This relation

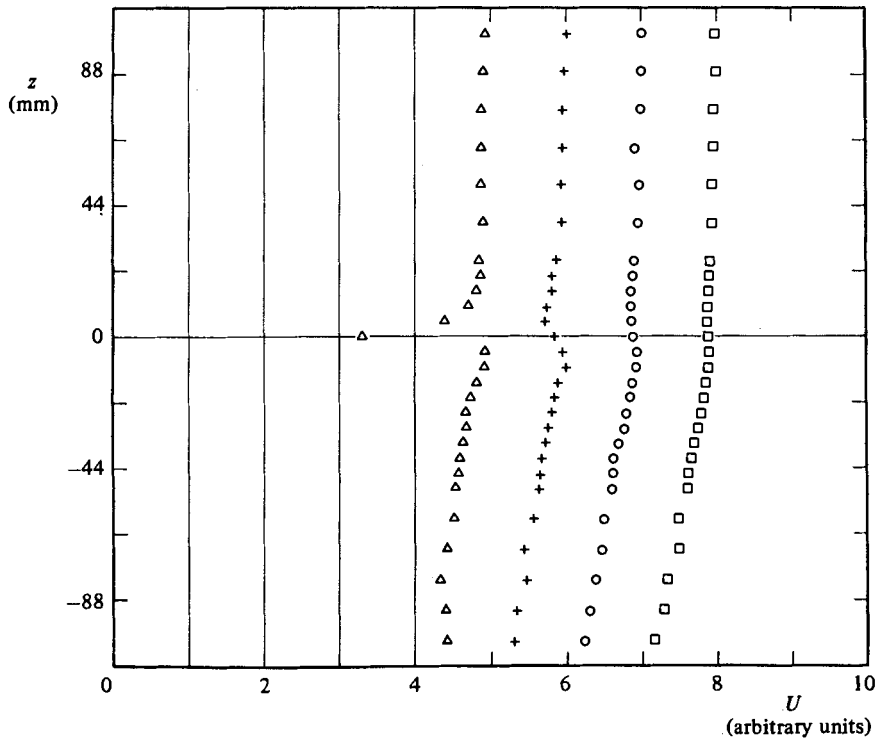

FIGURE 11. Mean-velocity profiles from experiment B; symbols as in figure 5.

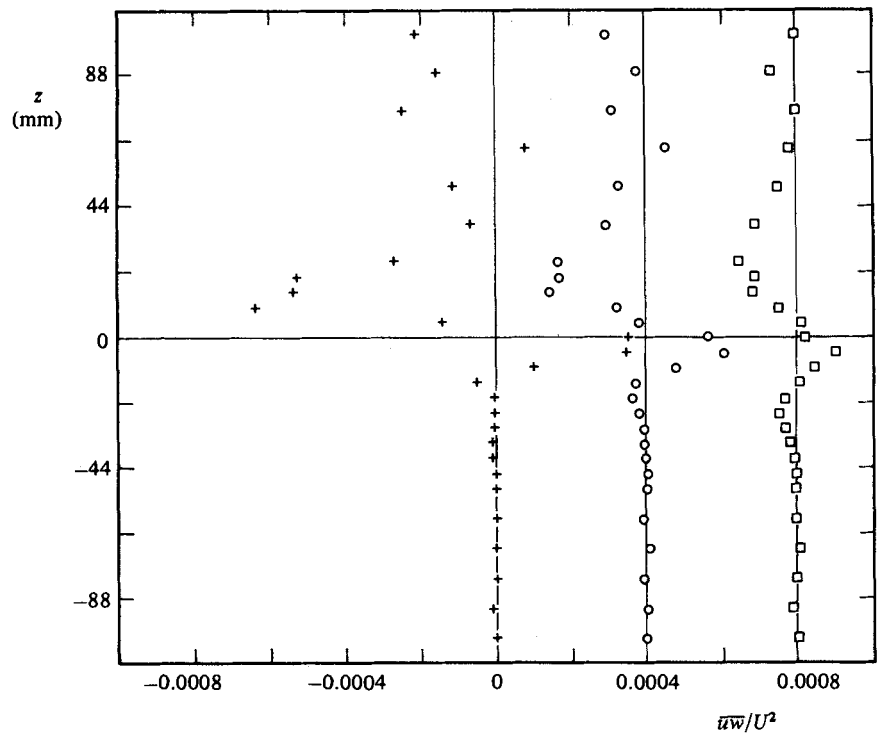

FIGURE 12. Measured distributions of turbulent shear stress for experiment B; symbols as in figure 5.

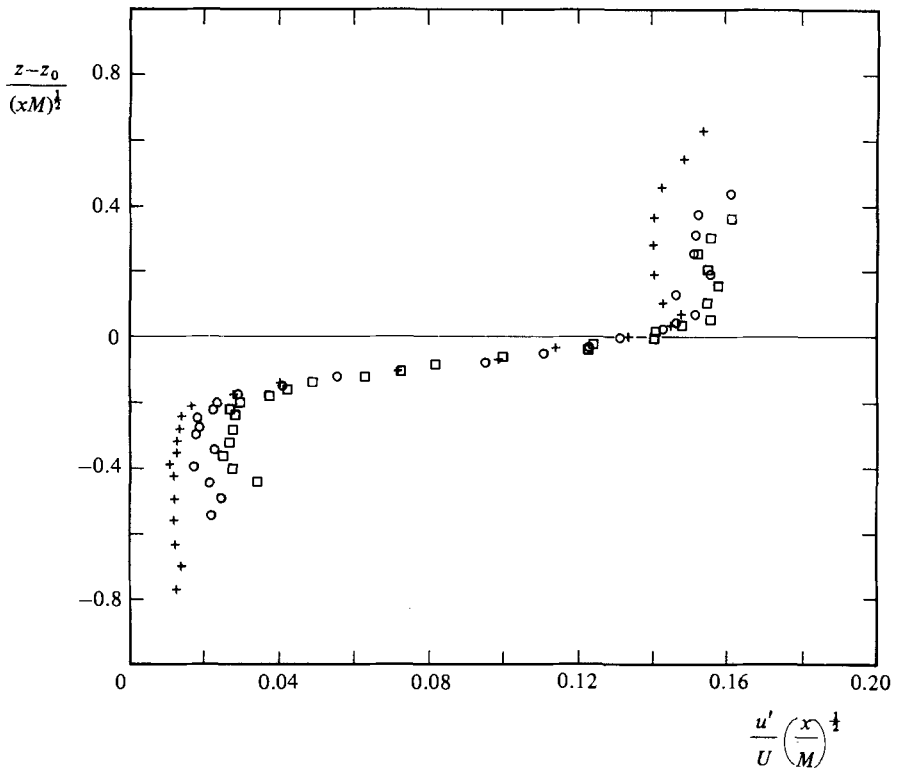

FIGURE 13. Self-similar plot of longitudinal turbulence intensity of experiment B based on scales appropriate to a small deficit wake; symbols as in figure 5.

between turbulence scale and wrinkle amplitude has been used in a previous study (Gartshore 1968) in which the large-eddy equilibrium hypothesis was examined for several self-preserving flows. Intermittency was clearly visible in the oscilloscope traces of the present experiment but was not measured explicitly. The effect of intermittency on time-averaged measurements is examined in §5.

The measurements of turbulent velocity of figures 6 and 7 can be plotted in a self-similar form by the use of conventional small-deficit wake scaling, in which lengthscales vary as $x^{\frac{1}{2}}$. Then plots of $(x^{\frac{1}{2}}u')$ and $(x\overline{uw})$ versus $(z-z_0)/x^{\frac{1}{2}}$ should place all the wake data on a single curve in each case, where the virtual origin is at z_0. The turbulence intensity and shear stress data at the three downstream stations (x = 0.38, 0.76 and 1.14 m) 'collapse' reasonably well (figures 9 and 10).

Similar results are found for experiment B, although now the mean velocity below the wake has a small but significant gradient, provided by the curved screens (see figure 11). Values of $(M/U)\,\mathrm{d}U/\mathrm{d}z$ are about 0.069, and become more uniform downstream of the plate. Intensities drop rapidly across the wake, as before. The shear stresses measured near the wake are plotted in figure 12 for experiment B. They are similar to those found for experiment A across most of the flow, showing positive and negative peaks associated with the wake. However, a small but important region of negative $\overline{uw}$ is found below the wake. This region is present in all profiles and can be seen to increase in extent and in magnitude (relative to the surrounding turbulence, which progressively decays) as x increases. Note that $\overline{uw}$ changes sign at about $z = -15$ mm for x = 750 and 1130 mm and that the mean velocity gradient

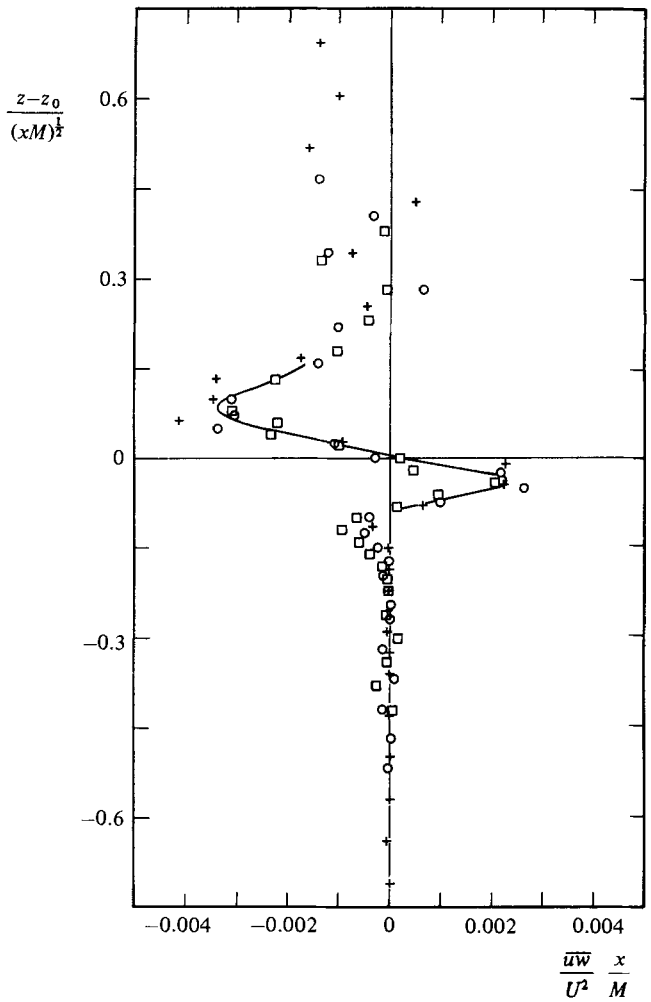

FIGURE 14. Self-similar plot of the shear stress distributions of experiment B based on scales appropriate to a small deficit wake; symbols as in figure 5.

decreases to zero at $z = -12$ to -16 mm for the same streamwise locations. We shall discuss this interesting effect later.

Wake scaling again provides a reasonable collapse for the data, as shown in figures 13 and 14, although there are important departures from self-similarity for the region below the wake in figure 14. These will be discussed later.

The data measured in this experiment cannot be compared directly with the theoretical results of §2 until some account has been taken of the intermittency. This effect is considered in §5.

5. The effects of intermittency

The effect of intermittency on time-averaged measurements made without using conditional sampling is to blur any rapid changes which may occur across the superlayer, and to average values measured inside and outside the boundary between the turbulent and irrotational motions. This effect can be described by first

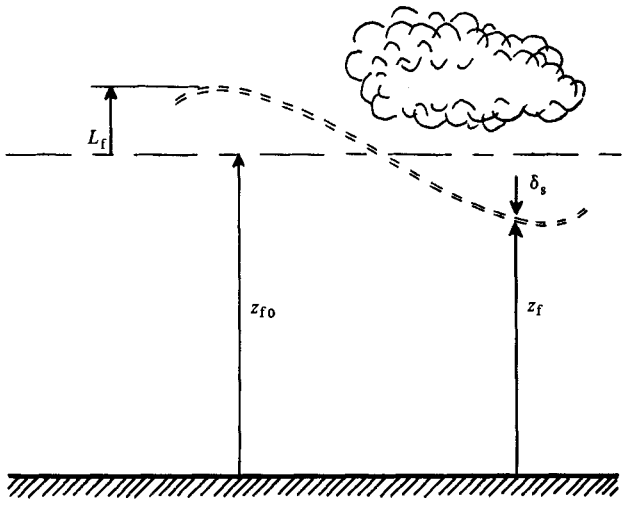

FIGURE 15. Sketch identifying symbols used in discussion of intermittency effects: = = = =, instantaneous front or 'superlayer'; – – – –, mean front position.

considering an interface between the two types of flow, which is located at $z = z_f$ as sketched in figure 15. Longitudinal intensities (or other time-average quantities) are given by

$$\overline{u^2} = u_\infty^2 f_1\left(\frac{z_f - z}{L_\infty}\right) \quad (z > z_f + \delta_s) \tag{19a}$$

in the turbulent region, and

$$\overline{u^2} = u_\infty^2 f_2\left(\frac{z_f - z}{L_\infty}\right) \quad (z < z_f - \delta_s) \tag{19b}$$

in the irrotational region, where u_∞^2 is the intensity and L_∞ is the longitudinal integral scale of the turbulence well above the interface. It is assumed that the thickness δ_s of the interface is very small compared with L_∞ (Townsend 1976, p. 211).

Now assume that the front moves such that the probability of z_f lying between z_f and $z_f + \mathrm{d}z_f$ is $p(z_f)\,\mathrm{d}z_f$ and that $p(z_f)$ is Gaussian, so that

$$p(z_f) = \frac{1}{\pi^{\frac{1}{2}}} \frac{1}{L_f} \mathrm{e}^{-\xi^2}, \tag{20}$$

where $\xi = (z_{f0} - z_f)/L_f$, and L_f is a measure of the wrinkle amplitude of the front, actually $\sqrt{2}$ times the standard deviation of the front from its mean position, which is denoted by z_{f0}.

The total contribution to $\overline{u^2}$ at a position z is then

$$\frac{\overline{u^2}}{u_\infty^2} = \int_{-\infty}^{z} f_1(z_1)\, p(z_f)\, \mathrm{d}z_f + \int_{z}^{\infty} f_2(z_1)\, p(z_f)\, \mathrm{d}z_f, \tag{21}$$

with $z_1 = (z_f - z)/L_\infty$. The first term represents the contribution to u^2 from inside the turbulent region, and the second term that from the irrotational region. The final distribution of $\overline{u^2}(z)$ is continuous even if $f_1(0) \neq f_2(0)$, that is even if there is a discontinuity in $\overline{u^2}$ across the original assumed plane front. The integrals of (21) can be expressed conveniently as

$$\frac{\overline{u^2}}{u_\infty^2} = \frac{1}{\pi^{\frac{1}{2}}} \int_{-\infty}^{0} f_1(z_1) \exp\left\{-\left(\frac{\xi_1 - z_1}{\alpha}\right)^2\right\} \mathrm{d}z_1 + \frac{1}{\pi^{\frac{1}{2}}} \int_{0}^{\infty} f_2(z_1) \exp\left\{-\left(\frac{\xi_1 - z_1}{\alpha}\right)^2\right\} \mathrm{d}z_1, \tag{22}$$

where

$$\alpha \equiv L_f/L_\infty,$$

$$\xi_1 - z_1 = \frac{z_{f0}-z}{L_\infty} - \frac{z_f - z}{L_\infty}$$

$$= \frac{z_{f0}-z_f}{L_\infty}$$

$$= \xi\alpha.$$

Suitable functions $f_1(z_1)$ and $f_2(z_1)$ are now substituted into the integrals of (4) to provide predictions of $\overline{u^2}$ and, in an entirely parallel manner, $\overline{uw}$. The analysis of §2, case (i) gives the function $f_2(z_1)$ for $z > \delta_s/L_\infty$ outside the thin 'super' layer whose thickness can be ignored on the scale of L_∞; the more restrictive results of case (ii) demonstrate how the smooth transition in $\overline{uw}$ occurs across the interface and suggests values of $f_2(z_1)$ likely for small strain ratios in the thin layer $|z_1| \ll 1$. For present predictions it is also necessary to have values of $f_1(z_1)$ for all $z_1 < 0$. These will be established by the wake flow adjacent to the shear region in the experimental case here so that, far from the interface, we may assume $\overline{u^2}/u_\infty^2 \geqslant 1$ and $\overline{uw}/u_\infty^2 \geqslant +0.4$. The latter is typical of turbulence near the point of maximum shear in the lower half of the wake. For comparison with experiments the detailed distribution very near the interface is probably unimportant and the following simple values for $f_1(z_1)$ have been used for all $z_1 < 0$:

$f_1(z_1) = 1$ for the longitudinal turbulence $\overline{u^2}$,

$f_1(z_1) = 0.4$ for the turbulent correlation $\overline{uw}$.

In addition the values of $f_2(z_1)$ calculated in §2, case (i), have also been used for $z_1 > 0$. The assumed distributions of $f(z_1)$ are therefore discontinuous at the interface, an approximation which is strictly incorrect as pointed out in §2, case (ii), but one which is not likely to affect the resulting trends significantly. Taking $f_1(z_1)$ as constant, the first integral of (22) can be expressed as a simple error function.

Values of L_f/L_∞, denoted here by α, can be estimated from previous measurements of intermittency in turbulent wakes (Gartshore 1966); they are found to be about 0.8, and values of 0.6, 0.8 and 1.0 have been used in the calculations to demonstrate the sensitivity of the resulting distributions to the size of this ratio.

The integrations described by (22), used with the computed results of figures 3(*a*, *b*), are plotted in figures 16 and 17 for $\overline{u^2}$ and $\overline{uw}$ respectively. Note that the sign of the shear stress $\overline{uw}$ is different on the two sides of the front, positive for $z_1 < 0$ (in the turbulent region) and negative or zero for $z_1 > 0$ (in the irrotational region) depending on the strain. Various overall strain ratios T are included in the plots of figures 16 and 17, including $T = 0$ and several values of α are used in the figures as already mentioned.

For the cross-stream intensity w^2, the analysis of §2 shows that there is no effect of strain and that this intensity is given for all T by the expression

$$\frac{\overline{w^2}}{u_\infty^2} = (1+2z_1)^{-4}$$

before considering intermittency. Because $\overline{u^2}/u_\infty^2$ at $T = 0$ is exactly one-half of this, the final distribution of $\overline{w^2}/u_\infty^2$ for all T is similar to that for $\overline{u^2}/u_\infty^2$ for $T = 0$, shown in figure 16 and including the effect of intermittency.

The result of Phillips (1955) and others, that $\overline{u^2} \propto (z-z_0)^{-4}$ is valid asymptotically

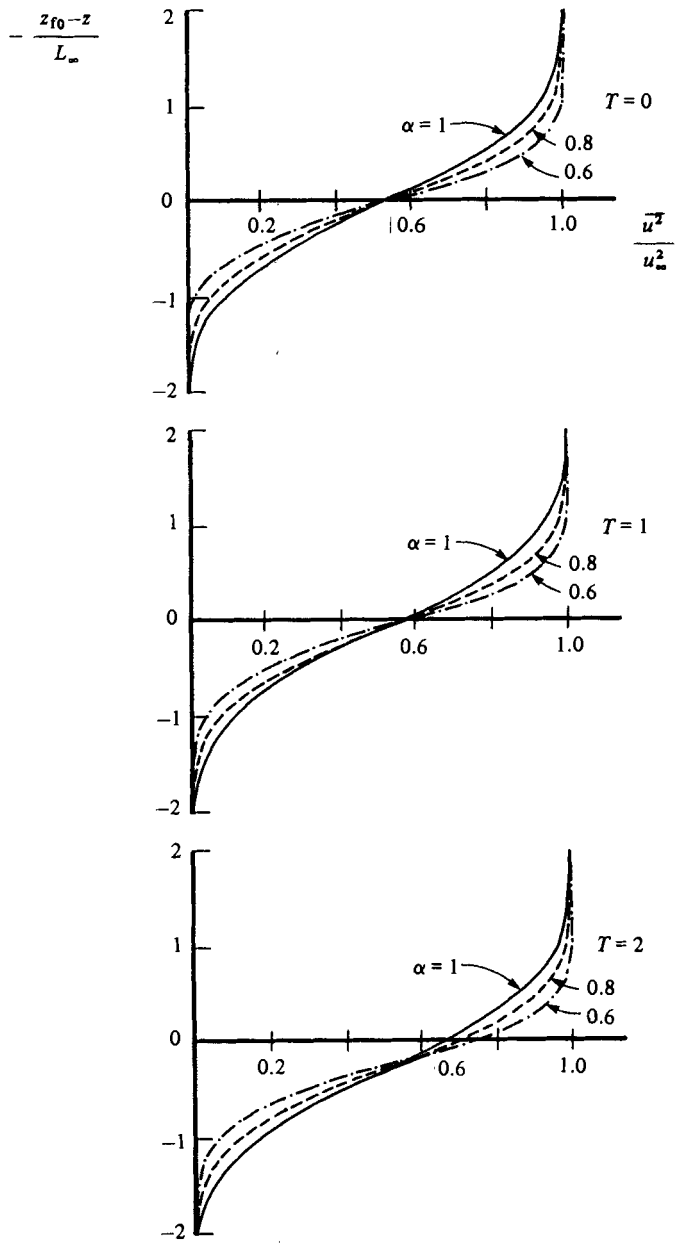

FIGURE 16. Calculated distributions of longitudinal fluctuation energy including the effect of intermittency.

for $T = 0$, even after intermittency has been included. This is illustrated in figure 18, where the results of the integration (taking $\alpha = 1$ for simplicity)

$$\frac{\overline{u^2}}{u_\infty^2} = \frac{1}{\pi^{\frac{1}{2}}}\int_{-\infty}^{0} e^{-(\xi_1 - z_1)^2}\,dz_1 + \frac{1}{\pi^{\frac{1}{2}}}\int_{0}^{\infty} \frac{0.5}{(1+2z_1)^4} e^{-(\xi_1 - z_1)^2}\,dz_1 \tag{23}$$

have been plotted as $(\overline{u^2}/u_\infty^2)^{-\frac{1}{4}}$ versus ξ_1. The region in which $(\overline{u^2})^{-\frac{1}{4}}$ is proportional to the distance from the average position of the turbulence front is clearly evident at large ξ_1. Small intensities of turbulence on the low turbulence side, which we might

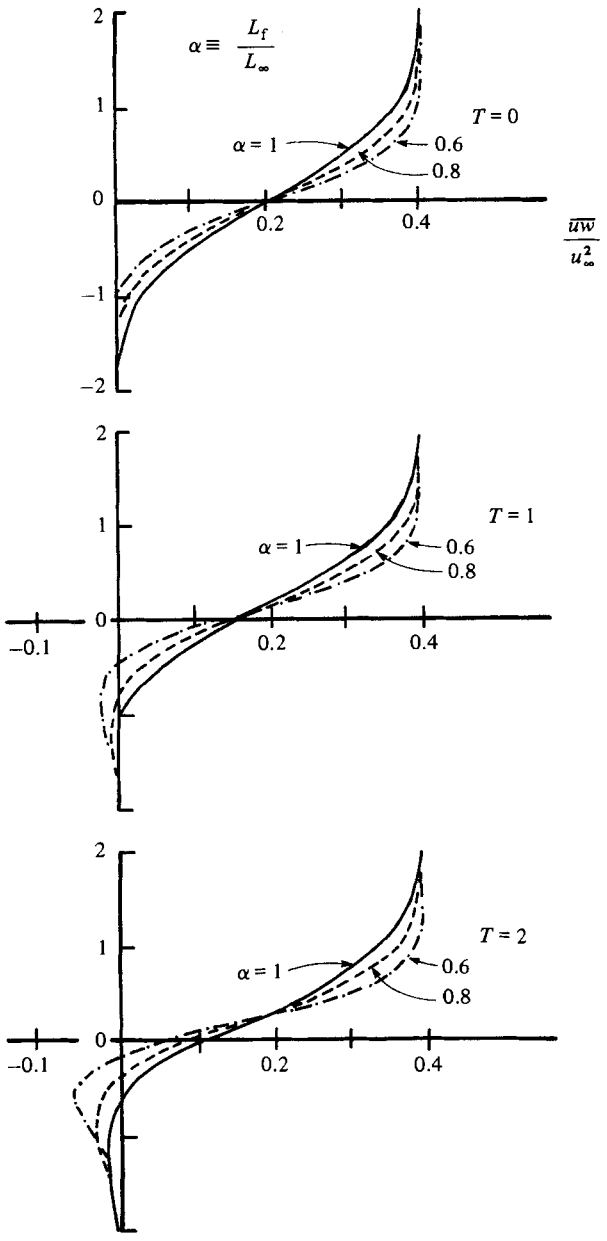

FIGURE 17. Calculated distributions of $\overline{uw}$ including effect of intermittency.

call freestream turbulence in this context, have a strong effect on this kind of plot, typically dominating the distribution before the theoretical asymptotic z^{-4} region is obtained. This is illustrated in figure 18 as well, where a freestream intensity u'_f one tenth of the turbulent intensity u'_∞ has been added. This curve rapidly approaches the value $(\overline{u_f^2}/u_\infty^2)^{-\frac{1}{4}}$, or $\sqrt{10}$ in this case, as $(z_{f0}-z)/L_\infty$ increases. A rather extensive region in which $\overline{u^2}$ is approximately proportional to z^{-4} appears in this curve, and it occurs at smaller values of $z_{f0}-z$ than in the case for which $\overline{u_f^2}=0$. Obviously various relative levels of freestream turbulence would move this region, its slope and its extent, giving an impression of changing turbulence scale. This effect of changing

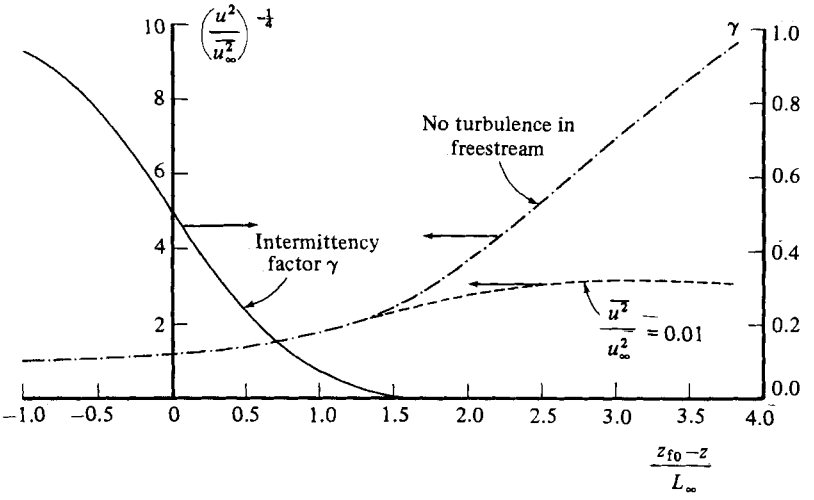

FIGURE 18. Calculated longitudinal fluctuation energy including effects of intermittency and freestream turbulence plotted to examine Phillips' hypothesis.

relative freestream intensity, is probably masking the actual changes in turbulence scale in the present data plot of figure 8, already mentioned. The curve of figure 18, which includes freestream turbulence, is obtained from

$$\frac{\overline{u^2}}{u_\infty^2} = \frac{1}{\pi^{\frac{1}{2}}}\int_{-\infty}^{0} e^{-(\xi_1-z_1)^2}\,dz_1 + \frac{1}{\pi^{\frac{1}{2}}}\int_0^\infty \left\{\frac{0.5}{(1+2z_1)^4} + \frac{u_f^2}{u_\infty^2}\right\} e^{-(\xi_1-z_1)^2}\,dz_1,$$

where the first integral on the right-hand side is equal to the intermittency factor γ, and is also plotted in figure 18. It is interesting to note that the asymptotic z^{-4} region appears in the case without freestream turbulence only when the intermittency has dropped to essentially zero whereas the approximate z^{-4} region which can be drawn when freestream turbulence is added appears where γ is as large as 0.2.

It must be emphasized that the results of figure 18 have been calculated by assuming that the probability distribution of the displacement of front is Gaussian, and that the wrinkle amplitude in the front L_f is equal to the longitudinal turbulence scale L_∞. Both assumptions influence the shapes of calculated curves in figure 18 and are used here for simplicity and illustration.

6. Discussion of results

The analysis presented in §2, and the subsequent integration for the effects of intermittency in §5, are based on some simplifying assumptions: the use of linear theory for f_2; the choice of ideal, constant values for $\overline{uw}$ and $\overline{u^2}$ inside the turbulent front; and the neglect of the effects of curvature of the turbulent front. Qualitatively, the experimental results of figure 14 agree with the predictions of figure 17, both showing regions of negative $\overline{uw}$ at small z for $T > 0$. The experimental strain ratio $(x/U)\,dU/dz$ is about 1.4 at the farthest downstream station (where $x/M \approx 20$), and is therefore in the range shown for the comparable quantity T in figure 17.

For a more-detailed comparison between prediction and theory, the scales L_∞ and u_∞^2 must be chosen appropriately for this experiment. As a first step, the velocity scale u_∞^2 is here taken to be the value of $\overline{u^2}$ at large z where the measured intensity is essentially independent of z. The lengthscale L_∞ is less obvious. The shear stress

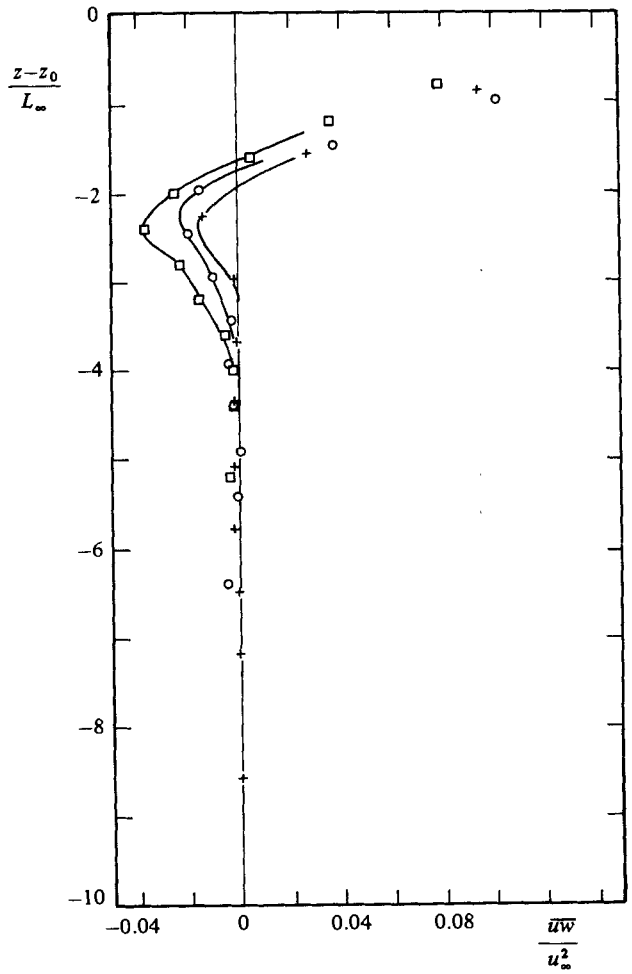

FIGURE 19. Measured values of shear stress in interaction region non-dimensionalized for comparison with the calculated distributions of figure 17 (experiment B); symbols as in figure 5.

plotted in figure 14 shows a wake-like character, with $\overline{uw}$ which is negative in the upper part of the wake (positive z) and positive in the lower part (negative z).

Assuming the scale of the lower part (which is less than that of the upper part) is the same as that of a simple wake, then on the basis of previous wake measurements the integral scale is given by $L/(xM)^{\frac{1}{2}} \approx 0.05$. Taking this as L_∞ for the present experiment, the measurements of $\overline{uw}$ in the important region where $\overline{uw}$ is negative can be rescaled into the theoretical non-dimensional form of figure 17. The results are shown in figure 19.

The maximum magnitude of the observed non-dimensional shear stress at the farthest downstream station is about 0.04 from figure 19. The predicted maximum magnitude (from figure 17) agrees with this experimental value if we choose $\alpha \approx 0.7$ for $T = 2$. In the experiment we have estimated α to be 0.8 and T to be 1.4, the first of these estimates being based on measurements of intermittency in simple turbulent wakes (Gartshore 1966). Thus the actual values of α and T are close to those required in the predictions to provide the observed maximum in the shear stress.

At the farthest downstream station ($x/M \approx 20$) the extent of the negative $\overline{uw}$ region is seen to be about $2L_\infty$ from the data of figure 19. The extent of the negative-$\overline{uw}$

region in figure 17 reaches about $1.6L_\infty$ for $T = 2$ and $\alpha = 0.7$, decreasing slightly for higher values of α or lower values of T. An important result of the theory, clearly present in the experimental observations, is that there can be an abrupt change of sign of Reynolds shear stress at a plane where the velocity gradient is non-zero. The prediction of small negative Reynolds stress induced in the uniform flow near this plane, while not observed explicitly in the present experiments, is not inconsistent with the measured results.

In general then, the magnitude and extent of the negative-$\overline{uw}$ region are similar in the analysis and in the measurements. Closer comparisons are not justified in the present case and better agreement could not be expected considering the assumptions necessary to make the comparison.

The chief conclusion from the present study is that irrotational fluctuations can create turbulent stresses in a region of mean-velocity gradients and that, for low strain ratios, this effect can be estimated using linear rapid-distortion theory. The effects are small in the longitudinal intensity and are most easily detected in the growth from zero of turbulent shear stress in the region affected. The effects of intermittency, inevitably present near the free boundaries of turbulent regions, are important in comparing predicted and measured results and further work, possibly involving higher strain ratios, should incorporate conditional sampling techniques to identify more clearly the processes inside and outside the fluctuating vorticity boundaries.

The experimental work reported here was completed while the first author was a visitor at DAMTP in Cambridge. Thanks are due to Mr David Cheesely for his help with construction of the apparatus and to others in DAMTP for this arrangement. Financial support for the work was received from the Killam Foundation and from an NSERC (Canada) grant. We are grateful to the referees for their comments.

REFERENCES

BRADSHAW, P. 1967 Irrotational fluctuations near a turbulent boundary. *J. Fluid Mech.* **27**, 209–230.

BRITTER, R. E., HUNT, J. C. R. & MUMFORD, J. C. 1979 The distortion of turbulence by a circular cylinder. *J. Fluid Mech.* **92**, 269–301.

CASTRO, I. P. 1976 Some problems concerning the production of a linear shear flow using curved wire-gauge screens. *J. Fluid Mech.* **76**, 689–709.

DURBIN, P. A. 1978 Rapid distortion theory of turbulent flows. Ph.D thesis, University of Cambridge.

GARTSHORE, I. S. 1966 An experimental examination of the large-eddy equilibrium hypothesis. *J. Fluid Mech.* **24**, 89–98.

GOLDSTEIN, M. E. 1979 Scattering and distortion of the unsteady motion on transversely sheared mean flows. *J. Fluid Mech.* **91**, 601–632.

HUNT, J. C. R. 1973 A theory of turbulent flow round bluff bodies. *J. Fluid Mech.* **61**, 625–706.

HUNT, J. C. R. & GRAHAM, J. M. R. 1978 Free-stream turbulence near plane boundaries. *J. Fluid Mech.* **84**, 209–235.

LACHMANN, G. V. (ed.) 1961 *Boundary Layer and Flow Control*, p. 1277. Pergamon.

MAULL, D. J. 1969 The wake characteristics of a bluff body in a shear flow. *AGARD CP* 48, *Paper* 16.

MEHTA, R. D., SHABAKA, I. M. M. A. & BRADSHAW, P. 1981 Imbedded longitudinal vortices in turbulent boundary layers. *Paper presented at Symp. on Numerical and Physical Aspects of Aerodynamic Flows, Col. State University, January 1981.*

TOWNSEND, A. A. 1976 *The Structure of Turbulent Shear Flow*, 2nd edn. Cambridge University Press.